Desalination and Water Treatment
www.deswater.com
doi: 10.1080/19443994.2013.803786

52 (2014) 4568–4582
June

Taylor & Francis
Taylor & Francis Group

Low-cost synthesis of mesoporous Zn(II)−Sn(II) mixed oxide nanoparticles for the adsorption of dye and heavy metal ion from aqueous solution

K. Yogesh Kumar[a], H.B. Muralidhara[a,*], Y. Arthoba Nayaka[b], J. Balasubramanyam[a]

[a]*Centre for Nanosciences, K.S. Institute of Technology, Visvesvaraya Technological University, Bangalore 560 062, India*
Tel. +91 9739315239; Fax: +91 80 28435723; email: hb.murali@gmail.com
[b]*School of Chemical Sciences, Department of PG Studies and Research in Chemistry, Kuvempu University, Shankaraghatta 577 451, India*

Received 16 August 2012; Accepted 23 April 2013

ABSTRACT

Mesoporous ZnO–SnO_2 mixed oxide nanoparticles (MMON) derived from precipitation method was investigated as a suitable adsorbent for the removal of malachite green oxalate (MGO) and hexavalent chromium (Cr) from waste water through batch adsorption process. The MMON was characterized by X-ray diffraction, scanning electron microscopy, tunneling electron microscopy, surface area analyzer, and FTIR spectroscopy. The effect of initial concentration, contact time, pH and adsorbent dose on the adsorption of MGO and Cr were studied. The Langmuir and Freundlich isotherm model was found to be more suitable to represent the experimental equilibrium isotherm results. The experimental kinetic data were a better fit with pseudo-second-order equation rather than pseudo-first-order equation. Thermodynamic studies indicated that adsorption process is endothermic in nature. The adsorption capacities of the MMON on MGO and Cr are found to be 189.7 and 5.9 mg g^{-1}, respectively. Regenerated MMON shows one-third of the original adsorption capacity. The results indicate that the synthesized MMON could be employed as a low-cost adsorbent for the removal of both MGO and Cr from the aqueous solution including industrial wastewater.

Keywords: Adsorption; Precipitation method; Mixed oxides; Regeneration

1. Introduction

Many industries, such as metal plating, mining, tanning, dye industries, textile, paper and plastics, generate huge amount of colored effluent and considerable amount of toxic metals into the environment, which has significant undesirable biological and ecological effects [1–5]. MGO and Cr are widely used in the above industries. The discharge of such effluents causes toxicological and esthetical problems. Exposure to Cr causes dermatitis, allergic skin reactions, and ulceration of intestine. It is a known carcinogenic agent [6,7]. The maximum permissible levels of Cr in potable and industrial wastewater are 0.05 and 0.25 mg L^{-1}, respectively [8]. Many adverse effects from the consumption

*Corresponding author.

1944-3994/1944-3986 © 2013 Balaban Desalination Publications. All rights reserved.

of the MGO due to its carcinogenic, genotoxic, mutagenic, and teratogenic properties in animal studies have been reported [8,9]. Thus, removal and remediation of this MGO and Cr from the industrial effluents is of significant environmental and commercial importance.

Several processes have been used and developed over the years to remove dissolved metals and dyes from industrial waste waters such as chemical precipitation [10], ion exchange [11], flocculation [12], reverse osmosis [13], membrane filtration [14], and adsorption. However, none of these methods has been widely used due to the relatively high-cost and low-feasibility for small-scale industries. Each process has its limitation in terms of cost or production of toxic derivatives. Among the techniques, adsorption technique offers significant advantages over the other removal techniques. The adsorption technique is more economical, simpler and is capable to efficiently treat dyes and heavy metal ions in their more concentrated forms. Also, adsorption techniques do not have secondary sludge disposal problems, making it environmental friendly. However, the adsorption process is the most promising technique and attracts the attention of many researchers in this field [15,16].

Among various adsorbents used, activated carbon is widely used as an efficient adsorbent for dye and heavy metal ion removal from aqueous solution owing to its excellent adsorption abilities, and it suffers from several drawbacks such as its high price both to the manufacturer and to the users. Hence, the alternative low-cost adsorbents like sepiolite [17], zeolite [18], waste metal hydroxide sludge [19], smectite [20], and bentonite [21] are some other adsorbents that have been used in this respect.

Recently, more attention was paid on mixed oxide nanoparticles as adsorbents due to its lower cost and higher adsorption capacity toward dyes and metals [22–25]. Among various mixed oxide nanoparticles, combination of ZnO and SnO_2 received special interests [26]. This mixed oxide possesses the characteristics of both components oxides and allow the possibility of tuning their materials properties as per the requirement for novel applications [27]. In the present study, an investigation has been carried out to check the reusability of MMON as a novel low-cost adsorbent to remove the MGO and Cr from synthetic wastewater. However, there is no literature on the adsorption of both heavy metal ion and dye using MMON as adsorbents.

Precipitation method to the synthesis of mixed metal oxide nanoparticles offer the possibility of better understanding and controlling the reaction pathways on molecular level, enabling the synthesis of nanomaterials with high crystallinity and well-defined uniform particle morphologies [28]. This study may helps to reduce the cost of waste disposal (recycling) and provide an alternative sorbent to the existing commercially activated carbon to remove the wastewater pollutants such as MGO and Cr. The influence of principal operational parameters of adsorption, such as the effect of initial concentration, adsorbent dose, influence of pH, and temperature, was monitored to optimize the sorption process for its possible use as a low-cost adsorbent in the field of wastewater treatment.

2. Materials and methods

2.1. Materials

All the reagents were of analytical grade and used as received without further purification. Zinc nitrate ($Zn(NO_3)_2.6H_2O$), tin chloride ($SnCl_2$), triton X-100 ($C_{14}H_{22}O(C_2H_4O)_n$), sodium hydroxide (NaOH), potassium dichromate ($K_2Cr_2O_7$) were purchased from SD Fine chemicals, Mumbai, India. MGO ($C_{52}H_{54}N_4O_{12}$) and 1,5-diphenyl carbazide ($C_{13}H_{14}N_4O$) (DPC) were purchased from Fisher Scientific India Pvt. Ltd., Mumbai and Loba Chemie. Pvt. Ltd., Mumbai, India, respectively. The stock solution (100 mg $L^{-1)}$ of Cr and MGO was prepared by dissolving stoichiometric amount of $K_2Cr_2O_7$ and malachite green oxalate in deionized water and further diluted to the desired concentrations for the experiments.

2.2. Preparation of Zn(II)–Sn(II) mixed oxide nanoparticles and characterization

Zn(II)–Sn(II) mixed oxide nanoparticles was prepared using the co-precipitation method. Zn $(NO_3)_2.6H_2O$ and $SnCl_2$ were used as the starting materials and NaOH as the precipitant. Zn $(NO_3)_2.6H_2O$ and $SnCl_2$ in a molar ratio of 1:1 were dissolved in 100 mL of deionized water, about 50 mL L^{-1} triton X-100 was added as capping agent which inhibits the anamolous growth of metal hydroxide crystals during the course of precipitation. The NaOH was added dropwise to the vigorously stirred mixed solution. Then, the resulting solution was kept at room temperature for about 3 h under constant stirring. The obtained slurry was centrifuged at 1,000 rpm, and precipitate was washed several times with water and alcohol, dried in an oven for a period of 1–2 h at 60˚C. Then, powder is further heated in silica crucible for a period of 6 h at 600˚C. Finally, the resulting adsorbent was stored in air tight container for further use to adsorption experiments.

X-ray diffraction (XRD) patterns were obtained on a Bruker D_2 Phaser XRD system. Surface morphology (SEM) was studied using scanning electron microscope (JEOL JSM 840). Transmission electron microscope (TEM) was recorded by using Philips CM-200 instrument. BET surface area, total pore volume, and average pore size of the MMON were measured using ASAP 2010 Micrometrics instrument by Brunauer–Emmett–Teller (BET) method. Finally, the Fourier transform infrared (FTIR) analysis was applied to determine the surface functional groups, using FTIR spectroscope (Bruker ATR), where the spectra were recorded from 400 to 4,000 cm^{-1}.

2.3. Batch equilibrium studies

To study the effect of parameters, such as initial concentration, contact time, adsorbent dose, solution pH, and temperature, for the removal of MGO and Cr on MMON were studied in duplicate by batch adsorption techniques in a 250 mL of stoppered flasks (Erlenmeyer flasks) that contain definite volume (100 mL in each flask) of fixed initial concentration of adsorbates. The experiments were carried out in thermostatic shaker at 200 rpm under room temperature, until equilibrium was reached. The resultant solutions were centrifuged, and the sample was analyzed by UV-vis spectrophotometer (Shimadzu UV-1650, Japan) at 617 and 540 nm, respectively, for MGO and Cr. The concentration of Cr was determined based on the color intensity Cr-DPC complex. The amount of adsorbate adsorbed at equilibrium condition, q_e ($mg\,g^{-1}$) and percentage removal efficiency R (%) were computed by Eqs. (1) and (2), respectively.

$$q_e = \frac{(C_0 - C_e)}{W} \times V \quad (1)$$

$$R\,(\%) = \frac{(C_0 - C_e)}{C_0} \times 100 \quad (2)$$

where C_0 and C_e are the initial and equilibrium concentrations ($mg\,L^{-1}$), respectively. V is the volume of solution (L) and W is the mass of adsorbent used (g).

2.3.1. Effect of initial concentration and contact time

MGO solutions with initial concentration of 10–40 $mg\,L^{-1}$ and Cr solutions with initial concentration 1–5 $mg\,L^{-1}$ were used in order to study the effect of adsorbates initial concentration and contact time on adsorption uptake. For the adsorption MGO and Cr for all the studies adsorbent dose was fixed 200 and 2,000 $mg\,L^{-1}$, respectively, and the solution pH was kept at 5 and 2.5, unless and otherwise mentioned.

2.3.2. Effect of adsorbent dose

To observe the effect of adsorbent dose on MGO, different amounts of adsorbents (200–800 $mg\,L^{-1}$) was added into 20 $mg\,L^{-1}$ initial concentration of MGO solution. To a 3 $mg\,L^{-1}$ of initial Cr solution, adsorbents doses were varied from 1,000–5,000 $mg\,L^{-1}$. The mixture was shaken at room temperature until the equilibrium time was reached. The initial concentration of MGO and Cr solution was kept 20 and 3 $mg\,L^{-1}$, respectively for all the studies.

2.3.3. Effect of solution initial pH

To study the effect of solution pH on MGO adsorption, 20 $mg\,L^{-1}$ of initial concentration at different pH values (2.0–12.0) was agitated with 200 $mg\,L^{-1}$ of adsorbents. The pH was adjusted with 0.1 N NaOH or 0.1 N HCl solution using pH meter. Percentage removal of Cr is not studied at higher pH. The literatures on Cr-DPC adsorption showed that maximum adsorption takes place in the pH range of 0.5–4, the coexisting Cr(VI) and Cr(III) can be separated, since Cr(VI) exists mainly in the anionic forms of ($HCrO_4^-$) and (CrO_4^{2-}) or ($Cr_2O_7^{2-}$). So in the determination of Cr(VI), pH was monitored in this range of acidity. It can be seen that when the pH is 2.5, there is a maximum adsorbed Cr-DPC intensity. Thus, this pH is preferred [29,30].

2.3.4. Effect of solution temperature

To study the effect of temperature on dye and metal ion adsorption characteristics, 20 $mg\,L^{-1}$ of initial concentration of MGO and 3 $mg\,L^{-1}$ of Cr were agitated with 200 and 2,000 $mg\,L^{-1}$ of adsorbents, respectively, at three different temperatures (30, 40, and 50 °C).

2.4. Regeneration of adsorbents

Dye and heavy metal loaded MMONs were regenerated by treating with 1 N CH_3COOH and 0.1 N NaOH solution, respectively, for about 1 h in digitally controlled water bath shaker in a beaker. Then, particles were filtered, washed several times with water, dried in an oven, and reused for adsorption studies.

3. Results and discussion

3.1. Characterization of adsorbent

Fig. 1 shows the XRD diffractograms of prepared MMON. All diffraction peaks can be perfectly indexed as the tetragonal rutile structure for SnO_2 and a hexagonal wurtzite structure for ZnO. No characteristic peaks for impurities, such as SnO, $ZnSnO_3$, and Zn_2SnO_4 were detected in the XRD pattern. It is reported that the ZnO always has larger grain size than SnO_2 at the same calcinations temperature and that the formation of ZnO crystallites was greatly restrained by the presence of SnO_2 [31]. Furthermore, the observed diffraction peaks are broad and less sharp, indicating that as prepared MMON with small dimension. The average crystallite size (D in nm) of MMON particles can be estimated according to the diffraction reflection by using Debye–Scherrer equation:

$$D_P = \left(\frac{K\lambda}{\beta_{1/2}\cos\theta}\right) \quad (3)$$

where K is a constant equal to 0.89, λ is the X-ray wave length equal to 1.54 A°, $\beta_{1/2}$ is the full width at half maximum and θ is the half diffraction angle. The phase compositions and size of MMON calculated according to XRD quantitative analysis from profile-fitting peaks were listed in Table 1.

Fig. 2 shows the typical SEM micrographs of MMON. It shows the interconnected ultrafine particles with nano-sized dimensions forming agglomerates, all the particles are irregular and some are spherical in nature. Size of the particles is also measured by SEM, the average particle size of MMON was found to be less than 10 nm. This indicates that the particle size of sample obtained by SEM observation is obviously bigger than the crystallite size determined by the XRD. This is not surprising because the particle size observed by SEM is the size of secondary (or aggregated) particles.

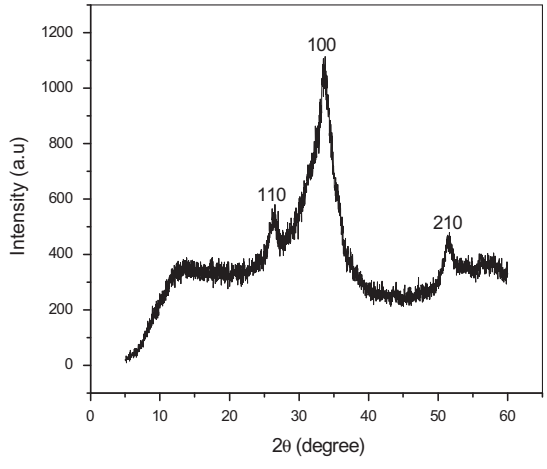

Fig. 1. Typical XRD pattern of MMON.

Table 1
Parameters derived from XRD analysis of MMON

Adsorbent	Phase	2θ	$h\ k\ l$	Size
MMON	SnO_2	26.30	(110)	3.38
	ZnO	32.44	(100)	5.42
	SnO_2	51.38	(210)	7.30

Fig. 3 shows the TEM micrographs of MMON, the shape was clear, and the aggregation was little. At the same time, TEM also showed that MMON were in nanometer scale and the sample was a crystalline in nature, which is in reasonable agreement with the results obtained from the XRD. Moreover, it was also easy to see from the TEM that the mean size of the synthesized particles was found to be less than 10 nm.

The nitrogen isotherms of the sample prepared were of type IV with hysteresis loop, which is a characteristic of mesoporous solids. MMON characterized by a pore distribution, sharply peaked in the mesoporous range between 7 and 20 nm as shown in Fig. 4. The average pore diameter and BET surface area of the MMON are found to be 14.18 nm and 26.31 $m^2\,g^{-1}$, respectively.

Fig. 5 shows the FTIR spectrum of MMON. The broad peak at the range of 3,428 cm^{-1} corresponds to the stretching vibration of –OH group. The peaks at 2,932 and 1,374 cm^{-1} are corresponds to the C–H and CH_2 stretching vibration of MMON sample. The peaks near 471 cm^{-1} agreed with stretching vibrations of Zn–O bonds [32]. The peak near 1,635 cm^{-1} can be assigned to the vibration of O–Sn–O that corresponds to the A2u mode [33], this will further confirms the formation of nanocomposites.

3.2. Effect of initial concentration and contact time

The amount of MGO and Cr adsorbed for different initial concentrations onto MMON is shown in Fig. 6. The adsorption process increases with time and then attains equilibrium value at a time of about 120 and 40 min, respectively. The removal was found to be dependent on the initial concentration; the amount adsorbed increasing with increase in initial concentration. Further, the time curve shows that the removal of MGO and Cr is rapid, but it gradually slows down until it reaches the equilibrium. At low concentrations, the ratio of available surface to the initial concentration is larger, so the removal becomes independent of initial concentrations. However, in the case of higher

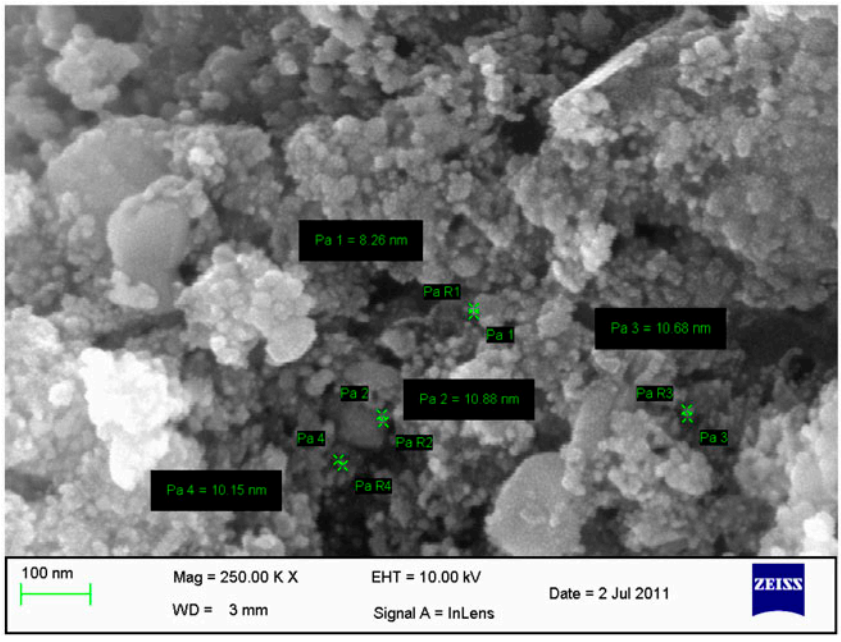

Fig. 2. Typical SEM micrograph MMON.

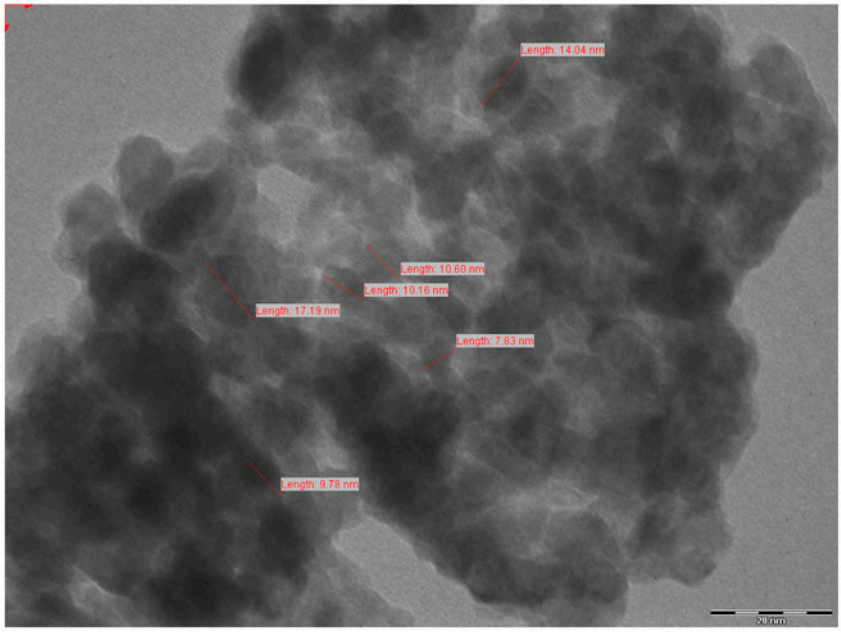

Fig. 3. Typical TEM micrograph MMON.

concentrations, this ratio is low; the percentage removal then depends upon the initial concentration and had only a small influence on the time of contact necessary to reach equilibrium [34]. On changing the initial concentration of MGO and Cr from 10 to 40 mg L^{-1} and 1 to 5 mg L^{-1}, the percentage removal decreased from 74.4 to 58.6 and 88.2 to 79.1, respectively, for a time period of 120 and 40 min.

3.3. Effect of adsorbent dose

Effect of adsorbent dose on percentage removal is shown in Fig. 7. Percentage removal increased from 68 to 81.6% for MGO and 78 to 91% for Cr and with increased in adsorbent dose from 200–800 mg L^{-1} and 1,000–5,000 mg L^{-1}, respectively. With increase in MMON dose, more active surface area was available

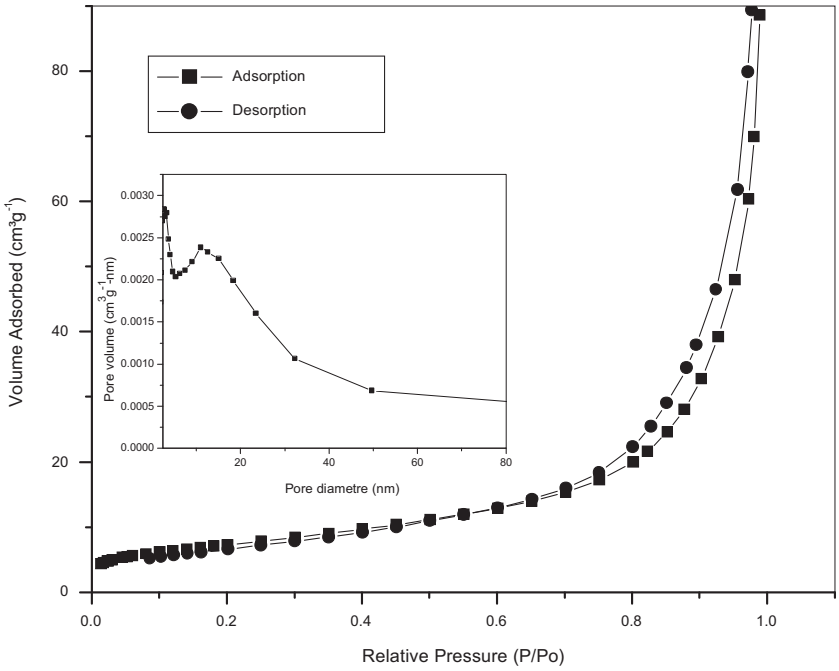

Fig. 4. Nitrogen adsorption–desorption isotherms (77 K); the inset figure shows pore size distribution of MMON.

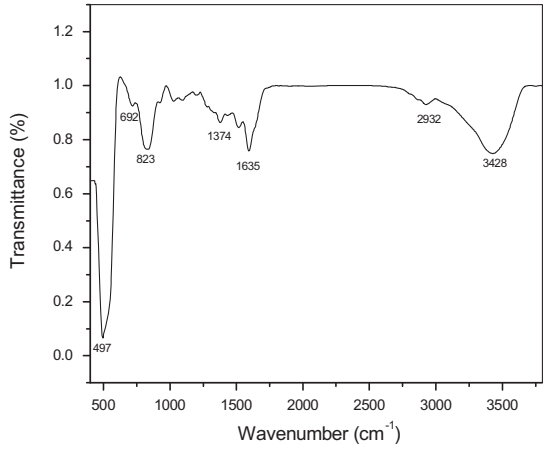

Fig. 5. FTIR spectrum of the MMON.

for bindings thus achieving an increase in removal percentage. However, reverse trend was observed with adsorbed MGO and Cr by unit amount of MMON (q_e). Once the interaction of MGO and Cr reached equilibrium, the addition of extra adsorbent was probably left unutilized or unsaturated. These unutilized mass of were accounted, however, during the calculation of removal capacity, leading to decrease in value of q_e [35].

3.4. Effect of pH

The effect of pH on percentage removal of dye was investigated over the range of pH values from 2 to 12. As shown in Fig. 8, the dye percentage removal is minimum at the initial pH 2. The percentage removal of dye adsorption increase when pH increases from 2 to 12, and then, the percentage removal dyes are not significantly altered beyond pH 8. It is well known that the surface of metal oxides or composites contain some oxygen groups such as hydroxyl groups (OH) and oxide groups after acid treatment [36]. At lower pH values, due to the protonation of electron π-rich regions on the surface of MMON, the positive surface charge can be formed. Under these conditions, the uptake of positively charged dyes will be low. When pH increases, the oxygen groups are ionized and the negative charge density on the surface increases, resulting in enhanced removal of dyes due to the electrostatic force of attraction between the negatively charged adsorbent surface and the positively charged cationic dyes [37].

3.5. Equilibrium adsorption isotherms

Analysis of isotherm data is important for predicting the adsorption capacity of the adsorbent, which is one of the main parameters required for the design of an adsorption system. Equilibrium isotherm studies were carried out with different initial concentrations of MGO (10–40 mg L^{-1}) and Cr (1–5 mg L^{-1}). Three models were used to analyze the equilibrium adsorption data: Langmuir, Freundlich, and Dubinin–Radushkevish (D–R) isotherm. Langmuir's model does not take into account the variation in adsorption

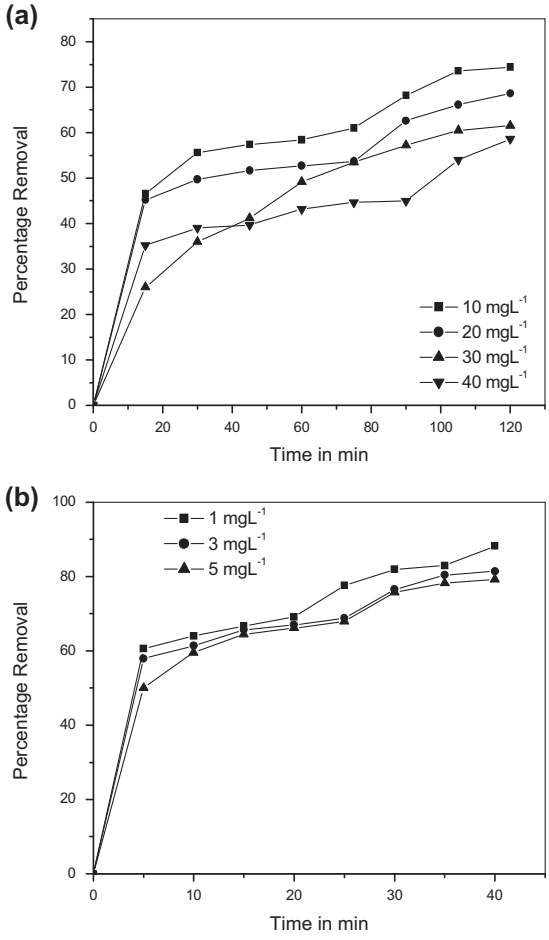

Fig. 6. Effect of contact time on adsorption of (a) MGO on MMON; (b) Cr on MMON at different initial concentrations.

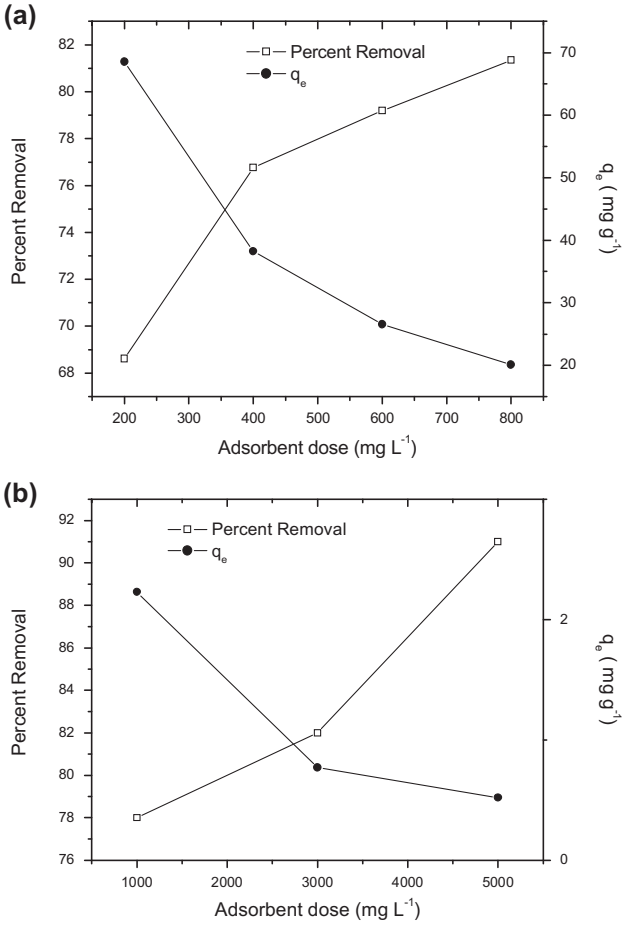

Fig. 7. Effect of adsorbent dosage on adsorption of (a) MGO on MMON; (b) Cr on MMON.

energy, but it is the simplest description of the adsorption process. It is based on the physical hypothesis that the maximum adsorption capacity consists of a monolayer adsorption, that there are no interactions between adsorbed molecules, and that of the adsorption energy is distributed homogeneously over the entire coverage surface interactive behavior between adsorbate and adsorbent.

The linear of Langmuir equation is given by:

$$\frac{C_e}{q_e} = \frac{1}{K_L} + \frac{a_L}{K_L} C_e \tag{4}$$

where C_e is the equilibrium concentration in ($mg\,L^{-1}$), q_e is the amount adsorbed per unit mass of adsorbent in ($mg\,g^{-1}$) at equilibrium concentration C_e. The constant K_L ($L\,mg^{-1}$) is the Langmuir equilibrium constant, and the $[K_L/a_L]$ gives the theoretical monolayer saturation capacity, Q_0. Therefore, a plot of C_e/q_e vs. C_e (Fig. 9) gives a straight line of slope a_L/K_L and intercepts $1/K_L$.

The essential feature of the Langmuir isotherm can be expressed in terms of a dimensionless constant separation factor (R_L) given by the following equation:

$$R_L = \frac{1}{1 + a_L C_e} \tag{5}$$

the values of R_L indicate the shapes of isotherms to be either unfavorable ($R_L > 1$), linear ($R_L = 1$), favorable ($0 < R_L < 1$) or irreversible ($R_L = 0$). The low values of R_L indicate that high and favorable adsorption and also indicated that the MMON is a suitable adsorbent for the adsorption of MGO as well as Cr ions from aqueous solutions. The Langmuir isotherm shows that the amount of adsorption increases as the concentration increases up to a saturation point. As long as there are available sites, adsorption will increase with increasing concentrations, but as soon as all of the sites are occupied, a further increase in concentrations

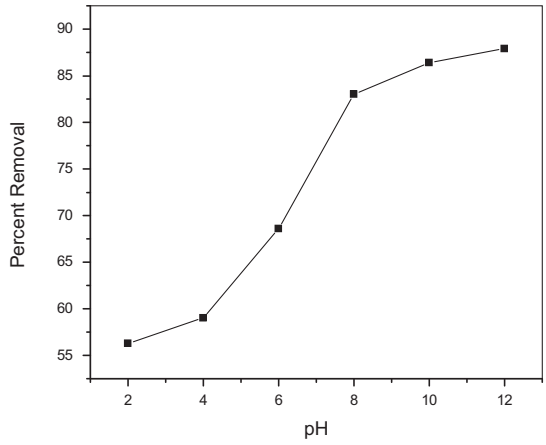

Fig. 8. Variation in percentage removal of MGO on MMON as a function of pH.

of solutions does not increase the amount of adsorbate on adsorbents [38]. The parameters of the Langmuir equation were calculated and are given in Table 2.

The Freundlich isotherm is derived by assuming a heterogeneous surface with a non-uniform distribution of heat of adsorption over the surface. This isotherm is suitable for a highly heterogeneous surface. The application of the Freundlich equation suggests that sorption energy exponentially decreases on completion of the sorptional centers of an adsorbent. The linear form of the equation is given by:

$$\log q_e = 1/n \log C_e + \log K_F \quad (6)$$

where K_F (mg g^{-1}), $1/n$ is the Freundlich adsorption constant and $1/n$ is a measure of the adsorption intensity. The linear plot between log q_e vs. log C_e (Fig. 10) gives a straight line with K_F and $1/n$ determined from the slope and intercept, respectively. The magnitude of exponent n indicates the favorability of adsorbent/adsorbate system where values of $n > 1$ represents favorable adsorption. The parameters of Freundlich equation for system studied are given in Table 2. The value of n indicates good adsorption over the entire range of concentration studied.

The Dubinin–Radushkevish (D–R) isotherm can be used to describe adsorption on both homogeneous

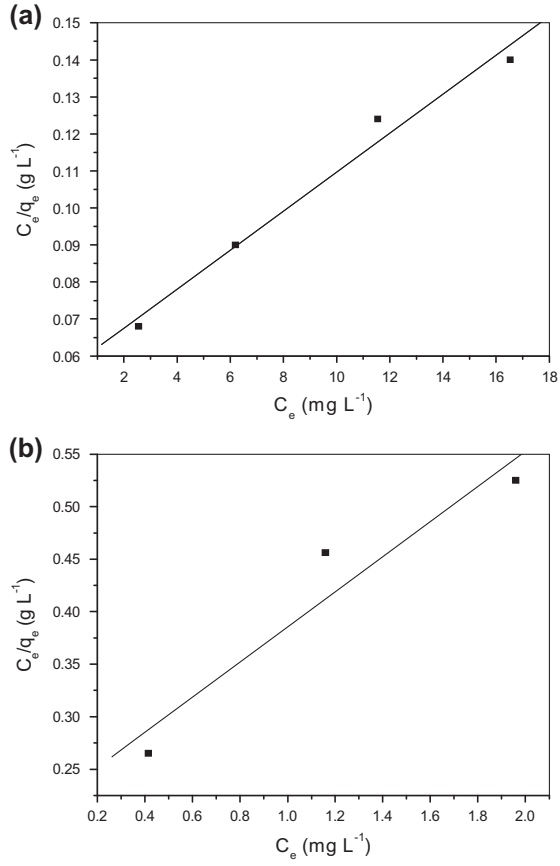

Fig. 9. Fits of the Langmuir adsorption isotherms for (a) MGO on MMON; (b) Cr on MMON.

and heterogeneous surface (Fig. 11). The model is often expressed as:

$$\ln q_e = \ln q_m - k\varepsilon^2 \quad (7)$$

where q_m is the D–R monolayer capacity (mmol g^{-1}), k is a constant related to the adsorption energy and ε is Polanyi potential which is related to the equilibrium concentration as follows:

$$\varepsilon = RT \ln\left(1 + \frac{1}{C_e}\right) \quad (8)$$

Table 2
Adsorption isotherm parameters of MGO and Cr adsorption on MMON

Metal ion	Langmuir isotherm			Freundlich isotherm			D–R isotherm		
	Q_0 (mg g^{-1})	K_L (L mg^{-1})	R^2	K_F (mg g^{-1})	n	R^2	q_m	E (kJ mol^{-1})	R^2
MGO	189.7	0.05	0.98	21.5	1.6	0.99	101.4	5.6	0.90
Cr	5.9	0.35	0.92	1.1	1.4	0.99	1.9	3.2	0.95

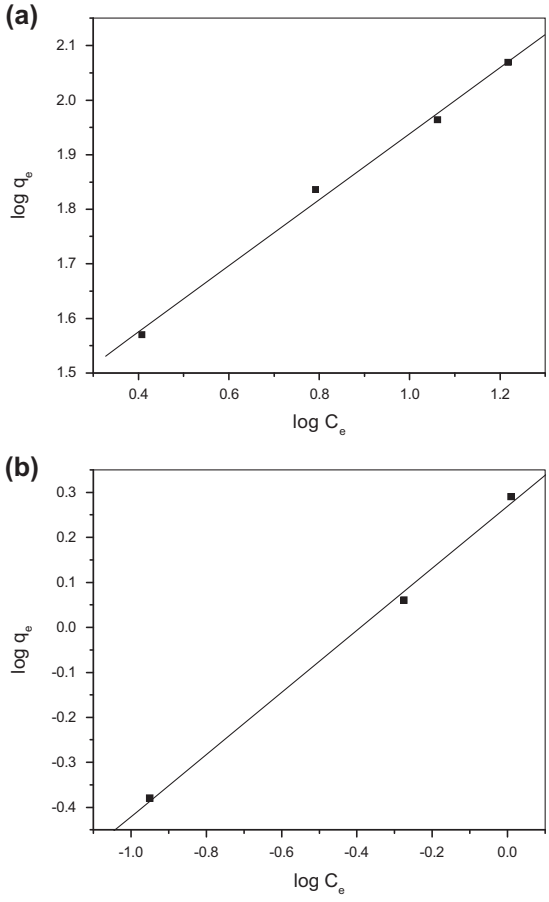

Fig. 10. Fits of the Freundlich adsorption isotherms for (a) MGO on MMON; (b) Cr on MMON.

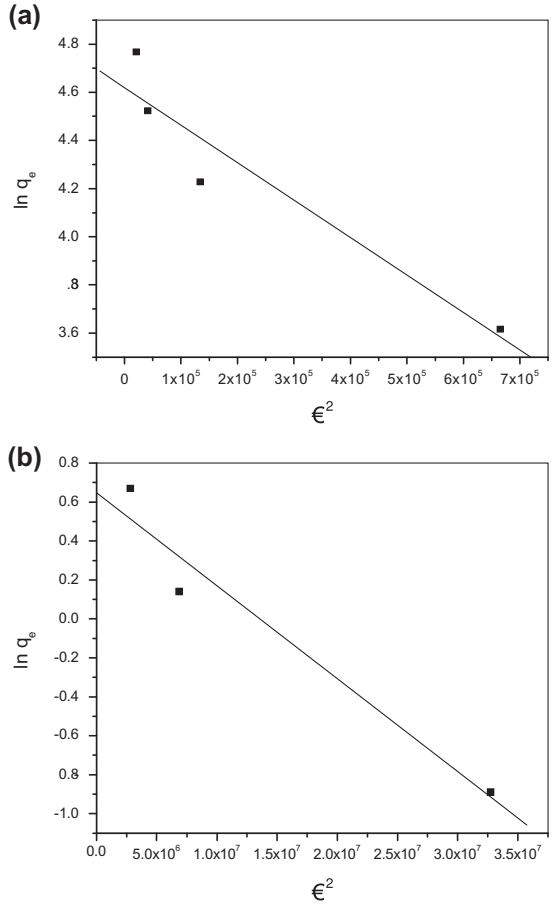

Fig. 11. Fits of the D–R adsorption isotherms for (a) MGO on MMON; (b) Cr on MMON.

where R is the gas constant ($8.314\,J\,mol^{-1}\,K^{-1}$) and T is the absolute temperature. The constant k gives the mean free energy E of adsorption per molecule of the adsorbate when it is transferred to the surface of the solid from infinity in the solution and can be computed using the relationship [39].

$$E = \frac{1}{\sqrt{2k}} \tag{9}$$

The magnitude of E is useful for estimating the mechanism of the adsorption reaction. In the case of $E < 8\,kJ\,mol^{-1}$, physical forces may affect the adsorption. If E is in the range of 8–16 $kJ\,mol^{-1}$, adsorption is governed by ion-exchange mechanism, while for the values of $E > 16\,kJ\,mol^{-1}$, adsorption may be dominated by particle diffusion [40]. Table 2 shows that the mean free energy was between 5.68 and $3.24\,kJ\,mol^{-1}$ for the studied MGO and Cr, respectively, which suggests that the sorption of MGO and Cr occurs via physisorption.

3.6. Adsorption kinetics

Two important physical–chemical aspects of the process, the kinetics and the equilibrium of adsorption were used to evaluate the process of adsorption. Two rate equations were used to analyze the adsorption kinetics data i.e. pseudo-first-order and pseudo-second-order reaction kinetics. The results are presented in Figs. 12 and 13 and Table 3. Lagergren's pseudo-first-order kinetics can be represented in linear form as:

$$\log(q_e - q_t) = \log q_e - \frac{k_1}{2.303}\,t \tag{10}$$

where q_e and q_t are the amounts of adsorbate adsorbed ($mg\,g^{-1}$) at equilibrium and at contact time t (min), respectively, and k_1 is the pseudo-first-order rate constant (min^{-1}). The first-order-rate constant k_1 can be obtained from the slope of the plot $\ln(q_e - q_t)$ vs. t. Linearized form of pseudo-second-order kinetics is given Eq. (11).

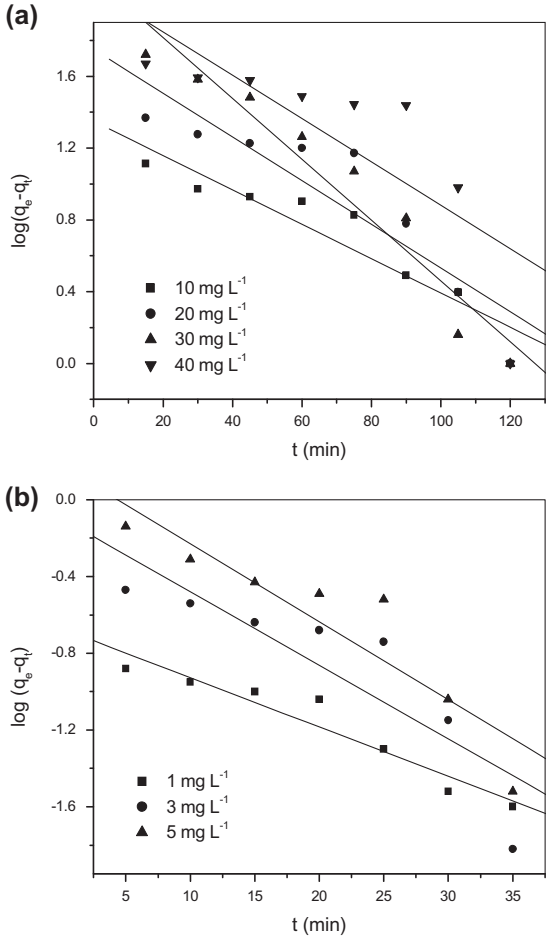

Fig. 12. Pseudo-first-order kinetic plots for the adsorption of (a) MGO on MMON; (b) Cr on MMON for different initial concentrations.

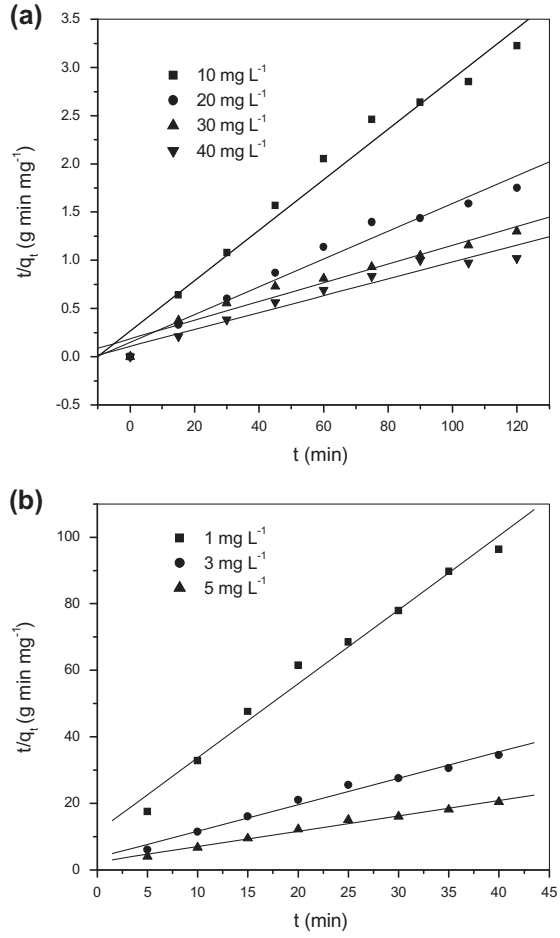

Fig. 13. Pseudo-second-order kinetic plots for the adsorption of (a) MGO on MMON; (b) Cr on MMON for different initial concentrations.

$$\frac{t}{q_t} = \frac{1}{k_2 q_e^2} + \frac{1}{q_e} t \tag{11}$$

where k_2 is the rate constant of the adsorption process ($g\,mg^{-1}\,min^{-1}$), q_e is the equilibrium amount of MGO and Cr adsorbed and q_t is the amount of MGO and Cr sorption at any time t ($mg\,g^{-1}$).

$$h = k_2 q_e^2 \tag{12}$$

where q_e is the equilibrium sorption capacity and k_2, the pseudo-second-order rate constant, can be determined experimentally from slope and intercept by plotting t/q_t against t [41]. The results obtained from applying the first-order kinetic model indicated that the correlation coefficients (R^2) values of fitting the first-order rate model are not high for the different MGO and Cr concentrations; furthermore, the estimated values of q_e calculated from the equation differed from the experimental values which show that the model is not appropriate to describe the adsorption process. However, the kinetics of MGO and Cr adsorption on MMON accords with the pseudo-second-order kinetic process correctly. Also, the plot showed an exact coefficient (R^2) which was coherent with the pseudo-second-order equation proposed. The calculated q_e values agreed very well with the experimental data. This is generally in agreement with other research's result that the pseudo-second-order model was able to describe properly the kinetic process of adsorption.

3.7. Intraparticle diffusion model

The most commonly used technique for identifying the mechanism involved in the adsorption process is

Table 3
Kinetics parameters for the adsorption of MGO and Cr on MMON

Kinetic models	Parameters	MGO concentration ($mg\,L^{-1}$)				Cr concentration ($mg\,L^{-1}$)		
		10	20	30	40	1	3	5
First-order kinetic model	$q_{e,cal}$ ($mg\,g^{-1}$)	22.4	56.2	143	122.9	0.2	1.2	1.5
	R^2	0.88	0.82	0.93	0.63	0.92	0.75	0.84
	$q_{e,exp}$ ($mg\,g^{-1}$)	37.2	37.2	68.6	92.2	0.4	1.1	1.9
Second-order kinetic model	$q_{e,cal}$ ($mg\,g^{-1}$)	38.2	69.4	103.0	114.5	0.4	1.2	2.1
	R^2	0.97	0.96	0.95	0.94	0.98	0.98	0.98
	$q_{e,exp}$ ($mg\,g^{-1}$)	37.2	68.6	92.2	117.3	0.4	1.1	1.9

by fitting the experimental data in an intraparticle diffusion plot. This model is significant because it is a rate-determining step in the liquid adsorption systems. The rate-limiting step (slowest step of the reaction) may be either the boundary layer (film) or the intraparticle (pore) diffusion of solute on the solid surface from bulk of the solution in a batch process. The probability of the intraparticle diffusion was explored by using the following equation suggested by Weber and Morries [42]:

$$q_t = k_{id}\, t^{1/2} + C \tag{13}$$

where q_t is the adsorption capacity at any time t and k_{id} ($mg\,g^{-1}\,min^{-1/2}$) is the intraparticle diffusion rate constant and C ($mg\,g^{-1}$) is the film thickness. Greater the value of C greater is the effect of boundary layer on adsorption process. If the rate-limiting step be the intra-particle diffusion, the plot of q_t against the square root of time should be a straight line and pass through the origin. The deviation of the plot from the linearity indicates the rate-limiting step should be boundary layer (film) diffusion controlled.

Multi linear plots of q_t vs. $t^{1/2}$ are presented in Fig. 14. Sharp first linear portion is due to the boundary layer (film) diffusion and the second linear one is for the pore diffusion. The nonlinearity of plots over a range of $t^{1/2}$ indicates multistage adsorption of MGO and Cr ions by MMON. The initial portion in the plots has attributed to the boundary layer effect or external mass transfer effect. The slope and intercept of the first portion of the plots has indicated the boundary layer (film) diffusion characteristics of the adsorption while that of the second linear portion is for the pore diffusion [43].

The values for $k_{id,1}$ and $k_{id,2}$ were computed from the slope of each plot. Table 4 gives the values of these parameters ($k_{id,1}$, $k_{id,2}$ and C). The values of $k_{id,1}$ were greater than that of $k_{id,2}$, and suggested that the boundary layer (film) diffusion had controlled the process of adsorption in the present case [44].

3.8. Thermodynamic studies

The thermodynamic parameters of the adsorption of MGO and Cr were determined using the following basic equations:

$$K_C = \frac{C_a}{C_b} \tag{14}$$

$$\Delta G^0 = -R\,T\,\ln K_C \tag{15}$$

$$\ln K_C = \frac{\Delta S^0}{R} - \frac{\Delta H^0}{R\,T} \tag{16}$$

where k_C is the distribution coefficient for the adsorption, ΔH^0 is the enthalpy change, ΔS^0 is the entropy change, ΔG^0 is the Gibb's free energy change, R is the gas constant, T is the absolute temperature, C_a is the MGO and Cr adsorbed per unit mass of the adsorbent, and C_b is the equilibrium adsorbate concentration in the aqueous phase. The values of ΔH^0 and ΔS^0 were determined from the slopes and intercept of the plot of ln K_c vs. ($1/T$) as shown in Fig. 15 and the values are listed in Table 5. The negative value of ΔG^0 at all temperatures indicate that the MGO and Cr adsorption reaction was spontaneous in nature and it was also observed that as the temperature increases, ΔG^0 decreases indicating the feasibility of adsorption at higher temperatures. So, it can be inferred that the reaction is spontaneous in nature [45]. As calculated ΔG^0 shows that adsorption process is predominantly a physical adsorption process. The calculated positive value of enthalpy demonstrated that the reaction was an endothermic process and so the reaction consumes

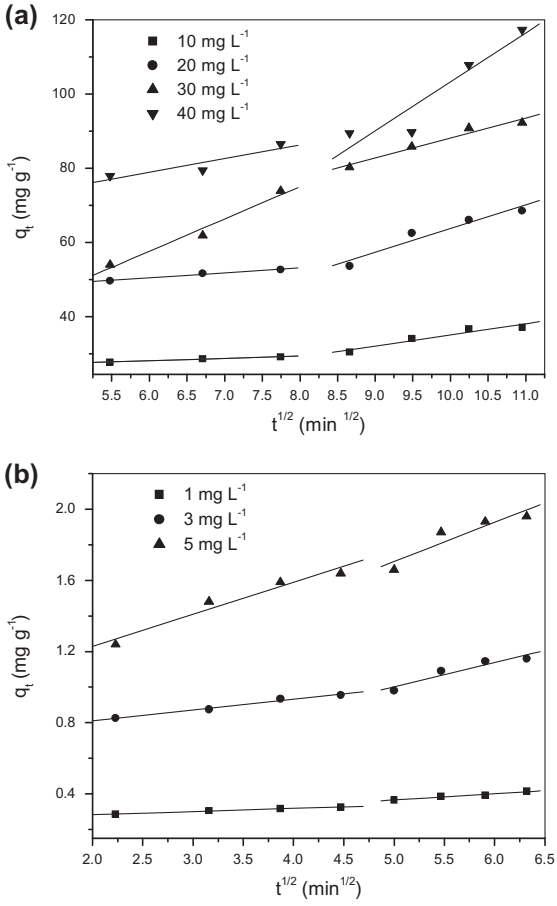

Fig. 14. Intraparticle diffusion model fitting of (a) MGO on MMON; (b) Cr on MMON.

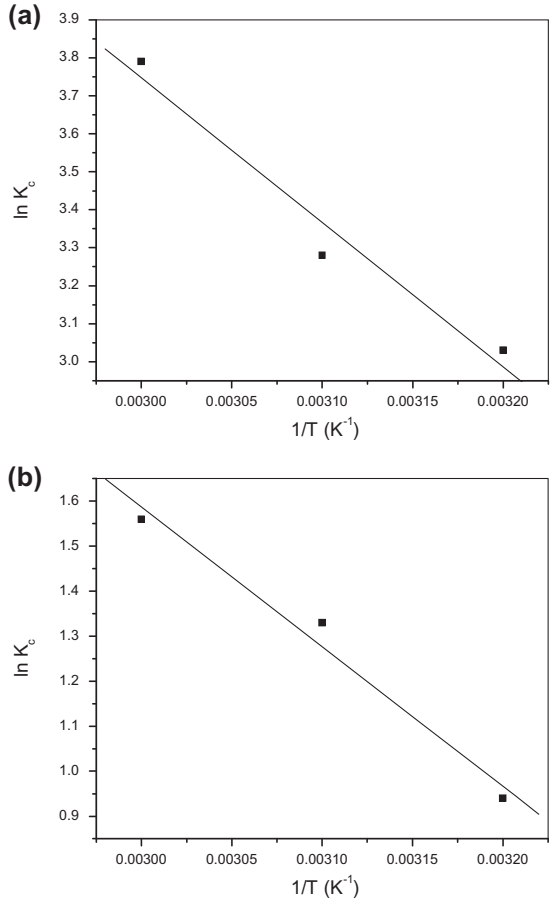

Fig. 15. Effect of temperature on adsorption of (a) MGO on MMON; (b) Cr on MMON.

energy the entropy of the reaction was positive as the displaced water molecules gain more translational entropy than was lost by the Cr ions and MGO, so as a result there will be increased randomness at the solid/solution interface.

3.9. Regeneration studies

Regeneration of adsorbents was carried out at optimum conditions i.e. 20 mg L^{-1} of initial concentration of MGO and 3 mg L^{-1} of Cr were agitated with 200 and 2,000 mg L^{-1} of adsorbents, respectively. The

Table 4
Intraparticle diffusion parameters for the adsorption of MGO and Cr on MMON

Kinetic model	Parameters	MGO concentration (mg L^{-1})				Cr concentration (mg L^{-1})		
		10	20	30	40	1	3	5
Intra particle diffusion model	C_1 (mg g^{-1})	0.62	1.33	3.69	8.70	0.01	0.06	0.18
	R_1^2	0.98	0.98	0.97	0.84	0.99	0.98	0.95
	$k_{id,1}$ (mg g^{-1} $min^{-1/2}$)	24.4	42.5	54.5	56.9	0.2	0.6	0.2
	C_2 (mg g^{-1})	3.01	6.36	5.37	13.7	0.03	0.13	0.22
	R_2^2	0.92	0.89	0.93	0.88	0.94	0.90	0.86
	$k_{id,2}$ (mg g^{-1} $min^{-1/2}$)	5.0	0.1	34.3	28.46	0.1	0.3	0.6

Table 5
Thermodynamic parameters for the adsorption of MGO and Cr on MMON

Parameters	MGO adsorption			Cr adsorption		
	Temperatures			Temperatures		
	30	40	50	30	40	50
ΔG^0 (kJ mol^{-1})	−7.6	−8.5	−10.1	−2.3	−3.4	−4.1
ΔH^0 (kJ mol^{-1})		−31.5			−25.7	
ΔS^0 (kJ mol^{-1} K^{-1})		0.12			0.09	

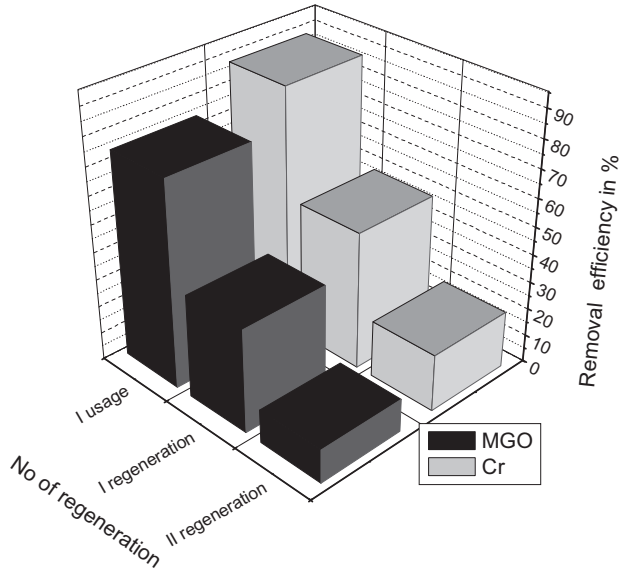

Fig. 16. Effect of regeneration of MMON on removal efficiency of MGO and Cr.

MGO adsorption is decreased from 74–12.1% (Fig. 16). Cr adsorption is also showed the similar pattern and adsorption is decreased from 88.2–20.6% with MMON (Table 6). As the number of regeneration increases, the poor efficiency of regenerated adsorbent in further adsorption studies is may be due to the strong interaction between the adsorbate and adsorbent, the number of active sites available on the surface of adsorbent decreases as the number of regeneration increases. The mechanism of desorption might be attributed to the replacement of H^+ and OH^- ions on the adsorbents.

Table 6
Regeneration parameters for adsorption of MGO and Cr on MMON

No. of regeneration	Removal % of MGO	Removal % of Cr
First usage	74.4	88.2
I regeneration	37.5	49.7
II regeneration	12.1	20.6

3.10. Comparison with other adsorbents

The comparison between the maximum adsorption capacities for MGO and Cr onto MMON and other adsorbents reported in the literature are given in Table 7. To the best of our knowledge, maximum adsorption capacity obtained in this study is comparable with the result from the reported adsorbents, so it is a real advantage that renders it becomes a suitable alternative for the cleanup of industrial effluents from the heavy metals.

Table 7
Comparison of monolayer maximum adsorption capacities of some adsorbents for MGO and Cr from aqueous solutions

Adsorbents	Adsorbate	Adsorption capacity (mg g^{-1})	References
Activated carbon (BBC)	MGO	20.7	[46]
Pine tree root decayed by brown-rot fungi (BRW)	MGO	42.6	[47]
Hydrilla verticillata biomass	MGO	69.8	[48]
MMON	*MGO*	*189.7*	Present study
Granular ferric hydroxide	Cr	0.7	[49]
Pine needles	Cr	5.36	[50]
Sugarcane bagasse pith	Cr	5.7	[51]
MMON	*Cr*	*5.9*	Present study

4. Conclusion

The entire experimentation concludes that MMON possess extremely good potential to remove both the waste materials. The effect of process parameters like contact time, initial concentration, adsorbent dose, pH, and temperature on adsorption of MGO and Cr was completely evaluated. The results obtained are well fitted in the linear forms of Langmuir, Freundlich and D–R adsorption isotherms. The Legergren first-order, Ritchie second-order kinetic and intraparticle diffusion models were used to explain the adsorption of MGO and Cr onto MMON. It was determined that interactions could best explained on the basis of the second-order kinetic model. The negative value of ΔG^0 at all temperatures indicate that the MGO and Cr adsorption reaction was spontaneous in nature, and it was also observed that as the temperature increases, ΔG^0 decreases indicating the feasibility of adsorption at higher temperatures. So, it can be inferred that the reaction is spontaneous in nature. Additionally, the MMON can be regenerated effectively by 1 N CH_3COOH and 0.1 N NaOH solution. All the results indicate that mixed metal oxide nanoparticles were promising sorbent for the removal of heavy metals as well as commercial dyes from contaminated waters.

Acknowledgments

The authors are grateful to Visvesvaraya Technological University for providing financial support under research grant scheme (Project No. VTU /Aca/ 2010-11/a-9/11353), The authors are also grateful to K.S. Institute of Technology, Bangalore for their support and IIT Kanpur, IIT Bombay and PPRI Bangalore for providing instrumental facilities.

References

[1] M. Mohapatra, S. Anand, Studies on sorption of Cd(II) on Tata chromite mine overburden, J. Hazard. Mater. 148 (2007) 553–559.
[2] B.L. Martins, C.C.V. Cruz, A.S. Luna, C.A. Henriques, Sorption and desorption of Pb^{2+} ions by dead Sargassum sp. biomass, Biochem. Eng. J. 27 (2006) 310–314.
[3] M.A. Rauf, S.M. Qadri, S. Ashraf, K.M. Al-Mansoori, Adsorption studies of toulidine blue from aqueous solutions onto gypsum, Chem. Eng. J. 150 (2009) 90–95.
[4] T. Robinson, G. McMullan, R. Marchant, P. Nigam, Remediation of dyes in textile effluent: A critical review on current treatment technologies with a proposed alternative, Bioresour. Technol. 77 (2004) 247–255.
[5] I.M. Banat, P. Nigam, D. Singh, R. Marchant, Microbial decolorization of textile-dye-containing effluents: A review, Bioresour. Technol. 58 (1996) 217–227.
[6] S. Hena, Removal of chromium hexavalent ion from aqueous solutions using biopolymer chitosan coated with poly 3-methyl thiophene polymer, J. Hazard. Mater. 181 (2010) 474–479.
[7] V. Neagu, S. Mikhalovsky, Removal of hexavalent chromium by new quarternized cross linked poly(4-vinyl pyridines), J. Hazard. Mater. 183 (2010) 533–540.
[8] S. Srivastava, R. Sinha, D. Roy, Toxicological effects of malachite green, Aquat. Toxicol. 66 (2004) 319–329.
[9] J.C. Sandra, R.B. Lonnie, F.K. Donna, R.D. Daniel, T. Louis, A.B. Frederick, Toxicity and metabolism of malachite green and leucomalachite green during short-term feeding to Fischer 344 rats and B6C3F1 mice, Chem. Biol. Interact. 122 (1999) 153–170.
[10] H. Cheng, Cu(II) Removal from lithium bromide refrigerant by chemical precipitation and electrocoagulation, Sep. Purif. Technol. 52 (2006) 191–195.
[11] S.A.A. Farha, A.Y.A. Aala, I.A. Ashourb, S.E. Garamona, Removal of some heavy metal cations by synthetic resin purolite C100, J. Hazard. Mater. 169 (2009) 190–194.
[12] M. Khayet, A.Y. Zahrim, N. Hilal, Modelling and optimization of coagulation of highly concentrated industrial grade leather dye by response surface methodology, Chem. Eng. J. 167 (2011) 77–83.
[13] S.K. Nataraj, K.M. Hosamani, T.M. Aminabhavi, Nanofiltration and reverse osmosis thin film composite membrane module for the removal of dye and salts from the simulated mixtures, Desalination 249 (2009) 12–17.
[14] Y. Cengeloglu, A. Torb, E. Kir, M. Ersoz, Transport of hexavalent chromium through anion-exchange membranes, Desalination 154 (2003) 239–246.
[15] L. Ai, H. Huang, Z. Chen, X. Wei, J. Jiang, Activated carbon/ $CoFe_2O_4$ composites: Facile magnetic performance and their potential application for the removal of malachite green from water, Chem. Eng. J. 156 (2010) 243–249.
[16] J.P. Chen, X.Y. Wang, Removing copper, zinc, and lead ion by granular activated carbon in pretreated fixed-bed columns, Sep. Purif. Technol. 19 (2000) 157–167.
[17] A. Ozcan, E.M. Oncu, A.S. Ozcan, Kinetics, isotherm and thermodynamic studies of adsorption of Acid Blue 193 from aqueous solutions onto natural sepiolite, Colloids Surf. A 277 (2006) 90–97.
[18] Y.E. Benkli, M.F. Can, M. Turan, M.S.C. Elik, Modification of organo-zeolite surface for the removal of reactive azo dyes in fixed-bed reactors, Water Res. 39 (2005) 487–493.
[19] S.C.R. Santos, V.J.P. Vilar, R.A.R. Boaventura, Waste metal hydroxide sludge as adsorbent for a reactive dye, J. Hazard. Mater. 153 (2008) 999–1008.
[20] F.L. Arbeloa, J.M. Herran Martinez, T.L. Arbeloa, I.L. Arbeloa, The hydrophobic effect on the adsorption of rhodamines in aqueous suspensions of smectites: The rhodamine 3B/Laponite B System, Langmuir 14 (1998) 4566–4573.
[21] A. Ozcan, C. Omeroğlu, Y. Erdoğan, A.S. Ozcan, Modification of bentonite with a cationic surfactant: An adsorption study of textile dye Reactive Blue 19, J. Hazard. Mater. 140 (2007) 173–179.
[22] A.I. Adel, A.E. Ayman, A. Ibrahim, M. Hideyuki, Heavy metal removal using SiO_2-TiO_2 binary oxide: Experimental design approach, Adsorption 14 (2008) 21–29.
[23] K.P. Gajendra, K.M. Parida, Fabrication of iron-cerium mixed oxide: An efficient photocatalyst for dye degradation, Int. J. Eng. Sci. Tech. 2 (2010) 53–65.
[24] L. William, I.V. Kostedt, A.I. Adel, W.M. David, Impact of heat treatment and composition of ZnO-TiO_2 nanoparticles for photocatalytic oxidation of an azo dye, Ind. Eng. Chem. Res. 47 (2008) 1483–1487.
[25] B. Krishna, B. Durjoy, C.G. Uday, Adsorption kinetics of fluoride on iron(III)-zirconium(IV) hybrid oxide, Adsorption 13 (2007) 83–94.
[26] A. Kandasami, Y.P. Jae, W.C. Sun, S.K. Sang, Nanocomposite ZnO–SnO_2 Nanofibers synthesized by electrospinning method, Nanoscale, Res. Lett. 5 (2010) 747–752.
[27] Z. Maolin, A. Taicheng, H. Xiaohong, W. Cun, Jiamo Preparation and photocatalytic properties of a nanometer ZnO–SnO2 coupled oxide, Appl. Catal. A 260 (2004) 215–222.

[28] L. Hua, Y.C. Chan, Y.P. Wu, B.Y. Wu, The determination of hexavalent chromium (Cr^{6+}) in electronic and electrical components and products to company with RoHS regulations, J. Hazard. Mater. 163 (2009) 1360–1368.
[29] J. Kotas, Z. Stasicka, Chromium occurrence in the environment and methods of its speciation, Environ. Pollut. 107 (2000) 263–283.
[30] S. Jambunath, P.K. Dasguptha, Determination of hexavalent chromium in leather extracts by the diphenyl carbazide (IU C-18) procedure: Pitfalls and refinements, JSL TC 84 (2000) 63–73.
[31] Y. Huaming, N. Sha, Freeze-drying synthesis and optical properties of nanocrystalline ZnO/SnO_2 composites, J. Optoelectron. Adv. Mater. 10 (2008) 197–200.
[32] V. George Chertihin, D. William Bare, L. Andrews, Reactions of laser-ablated chromium atoms with dioxygen: Infrared spectra of CrO, OCrO, CrOO, CrO3, Cr (OO) 2, Cr2O2, Cr2O3 and Cr2O4 in solid argon, J. Chem. Phys. 107 (1997) 2798–2807.
[33] S. Ardizzone, C.L. Bianchi, L. Borgese, G. Cappelletti, C. Locatelli, A. Minguzzi, S. Rondinini, A. Vertova, P.C. Ricci, C. Cannas, A. Musinu, Physico-chemical characterization of IrO_2–SnO_2 sol-gel nanopowders for electrochemical applications, J. Appl. Electrochem. 39 (2009) 2093–2105.
[34] H. Sufia, Removal of chromium hexavalent ion from aqueous solutions using biopolymer chitosan coated with poly 3-methyl thiophene polymer, J. Hazard. Mater. 181 (2010) 474–479.
[35] A.K. Potsangbam, R. Manabendra, C. Saswati, Adsorption behaviour of trivalent chromium on amine-based polymer aniline formaldehyde condensate, Chem. Eng. J. 149 (2009) 340–347.
[36] Z.K. Ji, D.L. Ai, Y. Xiang, F. Hai, Q. Wen, P. You, L. Hui, D. Wu, Photo-degradation of methylene blue using Ta-doped ZnO nanoparticles, J. Solid State Chem. 183 (2010) 1359–1364.
[37] Q. Song, H. Fei, Y. Shaoning, C. Gang, K. Jilie, Magnetic removal of dyes from aqueous solution using multi-walled carbon nanotubes filled with Fe_2O_3 particles, J. Hazard. Mater. 160 (2008) 643–647.
[38] A. Abbas, M. Razieh, Adsorptive removal of Congo red, a carcinogenic textile dye, from aqueous solutions by maghemite nanoparticles, J. Hazard. Mater. 174 (2010) 398–403.
[39] E. Bulut, M. Ozacar, I.A. Sengil, Adsorption of malachite green on to betonite: Equilibrium and kinetic studies and process design, Microporous Mesoporous Mater. 115 (2008) 234–236.
[40] I.H. Gubbuk, Isotherms and thermodynamics for the sorption of heavy metal ions onto functionalized sporopollenin, J. Hazard. Mater. 186 (2011) 416–422.
[41] Z. Yanmei, J. Qiang, Z. Tianwei, A. Yoshifumi, Adsorption of chromium(VI) from aqueous solutions by cellulose modified with-CD and quaternary ammonium groups, J. Hazard. Mater. 187 (2011) 303–310.
[42] T.G. Venkatesha, R. Viswanatha, Y. Arthoba Nayaka, B.K. Chethana, Kinetics and thermodynamics of reactive and vat dyes adsorption on MgO nanoparticles, Chem. Eng. J. 199 (2012) 1–10.
[43] V.K. Gupta, M.R. Ganjali, A. Nayak, B. Bhushan, S. Agarwal, Enhanced heavy metals removal and recovery by mesoporous adsorbent prepared from waste rubber tire, Chem. Eng. J. 197 (2012) 330–342.
[44] T. Sheela, Y.A. Nayak, Kinetics and thermodynamics of cadmium and lead ions adsorption on NiO nanoparticles, Chem. Eng. J. 191 (2012) 123–131.
[45] J. Hasanur, C. Debarati, S. Papita, A Study of the thermodynamics and kinetics of copper adsorption using chemically modified rice husk, Clean–Soil, Air, Water. 37 (2009) 704–711.
[46] S. Arivoli, M. Hema, P.M.D. Prasath, Adsorption of malachite green onto carbon prepared from borassus bark, Arabian, J. Sci. Eng. 34 (2009) 31–42.
[47] H. Zhang, Y. Tang, X. Liu, Z. Ke, X. Su, D. Cai, X. Wang, Y. Liu, Q. Huang, Z. Yu, Improved adsorptive capacity of pine wood decayed by fungi Poria cocos for removal of malachite green from aqueous solutions, Desalination 274 (2011) 97–104.
[48] R. Kannan, R. Rajasimman, M. Rajamohan, N. Sivaprakash, Equilibrium and kinetic studies on sorption of malachite green using hydrilla verticillata biomass, Int. J. Environ. Res. 4 (2010) 817–824.
[49] A.R. Asgari, F. Vaezi, S. Nasseri, O. Dordelmann, A.H. Mahavi, E. Dehghani, Removal of hexavalent chromium from drinking water by granular ferric hydroxide, Iran. J. Environ. Health Sci. Eng. 5 (2008) 277–282.
[50] S.P. Dubey, K. Gopal, Adsorption of chromium(VI) on low cost adsorbents derived from agricultural waste material: A comparative study, J. Hazard. Mater. 145 (2007) 465–470.
[51] U.K. Garg, M.P. Kaur, V.K. Garg, D. Sud, Removal of hexavalent chromium from aqueous solution by agricultural waste biomass, J. Hazard. Mater. 140 (2007) 60–68.